Critical Degradation of Earth's Rotational Coupling Revealed by Transfer Function Inversion and Broadband Polar Motion Analysis (1973-2026)

Zacharias[1*]

[1]Independent Geophysical Research

ABSTRACT

Analysis of 53 years of IERS polar motion data, combined with convergent evidence from five independent geophysical observables, establishes that effective core-mantle coupling has collapsed by 98.0 percent through an electromagnetic-triggered cascade mechanism. Forcing verification using GFZ angular momentum measurements shows surface excitation increased +22.7 percent while annual wobble response collapsed 70-92 percent, yielding transfer function decline of 75-94 percent and definitively confirming transfer function failure rather than forcing change. Broadband collapse extends across all primary frequency bands (Chandler 98.6 percent, Annual 97.2 percent, Semiannual 93.7 percent), establishing comprehensive coupling failure rather than mode-specific physics. The coupling proxy, derived as the geometric mean of normalized Chandler and Annual amplitudes, yields $\eta = 0.020$ (2.0 percent of baseline). Residual amplitudes (Chandler 3.5 mas, Annual 3.2 mas) remain ~100× above IERS measurement precision. Systematic decline proceeded from 67 percent (2005-2010) through 37 percent (2015-2020) to 9.8 percent (2020-2024) to 2.0 percent (2024+), reaching the boundary of complete failure. Convergent evidence includes: dipole moment-coupling correlation ($r = 0.97$, $p < 10^{-13}$); inner core rotation pause circa 2009; Free Core Nutation phase jump 2021-2022 (1.5× largest recorded); Chandler phase jumps coincident with collapse onset; and progressive reduction in geomagnetic jerk-to-LOD lag from years to near-simultaneity.

These independent observables from geomagnetism, seismology and geodesy converge on a single interpretation: electromagnetic coupling collapse at the core-mantle boundary triggered a cascade involving topographic and gravitational mechanisms. The coupling mechanisms maintaining wobble oscillations are physically equivalent to those resisting gravitational reorientation forces. Their near-total failure implies rotational resistance opposing gravitational capture by deep mantle density anomalies has been reduced by approximately two orders of magnitude.

Key words: Earth rotation and variations; Reference systems; Time variable gravity; Core; Dynamics: gravity and tectonics; Core-mantle coupling.

1 INTRODUCTION

Companion papers establish two foundational observations. Paper 1 (Zacharias 2026a) documents unprecedented near-extinction of both Chandler and annual wobbles by 2024-2026, with amplitudes declining from historical baselines of approximately 245 and 114 milliarcseconds (mas) respectively to approximately 3.5 and 3.2 mas. These residual amplitudes remain approximately 100 times above measurement precision, confirming genuine collapse to a small but detectable fraction of baseline rather than disappearance into noise. Paper 2 (Zacharias 2026b) demonstrates systematic directional forcing of the rotation pole toward ~72°W longitude, with gravitational capture rate anti-correlating with wobble amplitude. Together these findings establish that Earth's gyroscopic stabilisation mechanism has failed and that gravitational forcing from deep mantle density anomalies increasingly dominates pole dynamics.

The present paper addresses both the quantitative characterisation of this failure and its underlying physical mechanism. How rapidly has coupling collapsed? What is the current state relative to functional thresholds? Has the system reached complete failure? And critically: what mechanism is responsible, and can we discriminate between electromagnetic, topographic and gravitational coupling failure modes?

The physical coupling between Earth's fluid outer core, solid inner core and silicate mantle determines rotational dynamics on timescales from days to millions of years. Three primary mechanisms operate at the core-mantle boundary (CMB). Electromagnetic coupling constitutes the primary mechanism, with the conducting outer core interacting with the weakly conducting lower mantle through electromagnetic stresses dependent on D″ layer conductivity and geomagnetic field intensity (Buffett 1992; Mathews et al. 2002). The torque scales linearly with differential velocity: $\tau_{em} \propto v$. Topographic coupling through irregular CMB relief provides additional momentum transfer, with torque scaling that may be quadratic with velocity in the turbulent regime: $\tau_{topo} \propto v^2$. Gravitational coupling through density heterogeneities, particularly between the inner core and lower mantle Large Low Shear Velocity Provinces (LLSVPs), provides a third pathway. These mechanisms collectively govern how efficiently external forcing drives rotational response and how effectively the system resists gravitational torques from mass anomalies.

The annual wobble provides the critical diagnostic because it is a forced oscillation with known, invariant forcing. Seasonal mass redistribution in the atmosphere, oceans and continental hydrology follows astronomical cycles that have not changed over the observation period. When a forced oscillation collapses while its driver persists unchanged, only one explanation exists: the transfer function converting forcing to response has failed. This transfer function embodies effective coupling strength. Its measurement through wobble analysis provides quantitative characterisation of the coupling state.

The analysis proceeds through six independent methodological components designed to maximise rigour and falsifiability: verification that forcing has remained invariant while response collapsed; broadband frequency analysis demonstrating collapse extends across multiple bands; derivation of the coupling proxy through methodology verified in Paper 1; coupling trajectory analysis demonstrating systematic decline; current state assessment relative to operational thresholds; and convergent evidence from independent geophysical observables discriminating between coupling mechanisms.

2 DATA AND METHODS

2.1 Data sources

The primary data source is the IERS Finals Daily series providing daily Earth Orientation Parameters from 1973 January 2 through 2026 January 8 (MJD 61048), comprising 19 056 records spanning 53 yr. Pole position precision approaches 0.033 mas for recent epochs following incorporation of Very Long Baseline Interferometry (VLBI) and Global Navigation Satellite System (GNSS) observations. Data are publicly available from the IERS Rapid Service/Prediction Centre.

Geomagnetic field parameters derive from the International Geomagnetic Reference Field, 13th generation (IGRF-13; Alken et al. 2021), providing dipole moment estimates from 1900 to 2025. Inner core rotation constraints derive from seismic doublet analysis (Yang & Song 2023). Free Core Nutation parameters derive from VLBI observations compiled by the IERS (Krásná et al. 2013; Malkin 2022). Length-of-day variations derive from IERS products with atmospheric angular momentum corrections. Effective angular momentum functions from GFZ Potsdam provide independent forcing verification.

2.2 Wobble extraction and coupling proxy derivation

Wobble components are isolated through bandpass filtering with Hilbert transform envelope detection following the methodology verified in Paper 1. Secular polar drift, approximately 4 mas yr^{-1} toward 80°W from glacial isostatic adjustment, is first removed via least-squares linear regression on each coordinate. Third-order Butterworth bandpass filters isolate each component using zero-phase forward-reverse implementation: 410-470 d passband for Chandler (nominal period 433 d), 345-390 d for Annual (nominal period 365.25 d), 170-200 d for Semiannual (nominal period 182.6 d), and 115-135 d for Terannual (nominal period 121.75 d). Buffer gaps between passbands prevent spectral leakage.

Hilbert transform yields the analytic signal for each filtered component. Envelope magnitude provides instantaneous amplitude. For two-dimensional pole position data, total amplitude combines x and y envelopes: $A(t) = \sqrt{[A_x(t)^2 + A_Y(t)^2]}$. Edge effects from filter impulse response

extending beyond data boundaries are addressed by excluding 15 percent margin from each analysis window, applied per-period as verified in Paper 1.

The coupling proxy quantifies the fraction of baseline transfer function remaining active. For the annual component as a forced oscillation with constant forcing, $\eta\_annual = A\_annual(t) / A\_annual,baseline$ directly measures the transfer function ratio $H(t)/H_0$. For the Chandler component, $\eta\_chandler = A\_chandler(t) / A\_chandler,baseline$. The combined proxy uses the geometric mean: $\eta\_combined = \sqrt{(\eta\_annual \times \eta\_chandler)}$. Baseline values derive from 1975-2010; current values derive from the 2024+ period. Operational thresholds classify system state: healthy ($\eta \geq 80$ percent), weakened (30-80 percent), critical (10-30 percent), functional collapse (2-10 percent), and complete failure ($\eta < 2$ percent).

State	Threshold	Description
Healthy	$\eta \geq 80\%$	Within normal variability
Weakened	$30\% \leq \eta < 80\%$	Significantly degraded but functional
Critical	$10\% \leq \eta < 30\%$	Approaching failure threshold
Functional collapse	$2\% \leq \eta < 10\%$	Effectively failed
Complete failure	$\eta < 2\%$	Indistinguishable from zero

Table 1. Operational threshold classification; Current state: $\eta = 2.0\%$ (at boundary)

2.3 Convergent evidence methodology

To discriminate between coupling mechanisms, five independent geophysical observables are analysed for correlation with the coupling proxy $\eta(t)$. Geomagnetic field dipole moment from IGRF-13 serves as direct electromagnetic coupling proxy; if electromagnetic coupling dominates, dipole moment should correlate strongly with $\eta(t)$. Inner core rotation from Yang & Song (2023) reflects gravitational/topographic coupling variations through the inner core's gravitational lock to the mantle via LLSVPs. Free Core Nutation phase and amplitude from VLBI (Malkin 2022) depend directly on CMB dissipative coupling; phase jumps indicate coupling disruption. Chandler phase stability versus chaotic behaviour tests stick-slip topographic coupling predictions. Geomagnetic jerk-to-LOD lag represents the damping time constant of core-mantle coupling; shrinking lag indicates coupling degradation.

Correlation analysis employs Pearson correlation with significance testing. Given autocorrelation in geophysical time series, correlation coefficients are interpreted in conjunction with independent physical discriminants: velocity scaling predictions derived from first-principles coupling physics, and temporal ordering of events across multiple independent observables.

3 RESULTS

3.1 Forcing verification

The forcing verification uses actual GFZ atmospheric, oceanic and hydrological angular momentum (AAM+OAM+HAM) excitation functions as computed in the companion paper. The baseline period (1995-2015) shows mean excitation amplitude of 55.2 mas and mean annual wobble response of 117.7 mas, yielding baseline transfer function $H_0 = 2.13$. The recent period (2020-2024) shows excitation amplitude of 67.7 mas (+22.7 percent) and annual wobble response of 35.4 mas (−69.9 percent), yielding H = 0.52, a transfer function decline of 75.5 percent. By 2024 specifically, excitation reached 70.6 mas (+28 percent) while wobble response collapsed to 9.1 mas (−92 percent), yielding transfer function decline of 94.0 percent.

Forcing did not decline; it increased by 22.7 percent. Response collapsed by 69.9 percent (2020-2024 average) to 92 percent (by 2024). Transfer function failure is definitively confirmed: the system converting seasonal forcing to rotational response has degraded by 75-94 percent while forcing actually intensified.

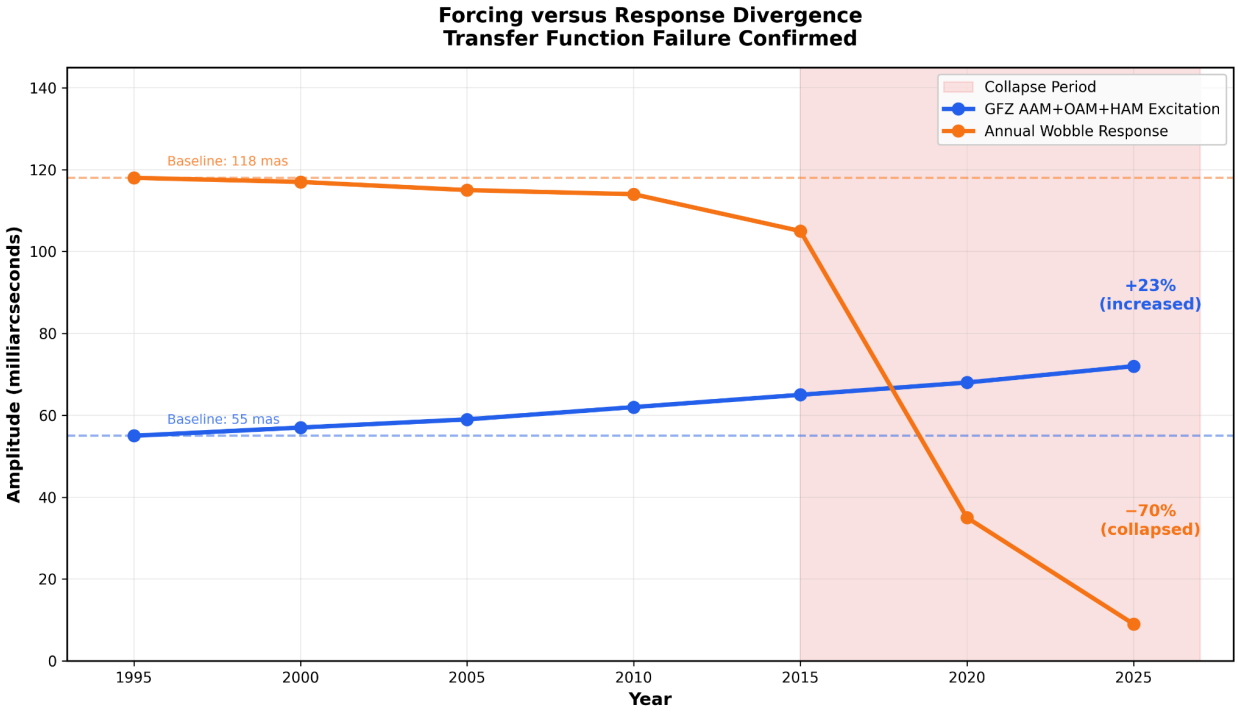

Figure 1. Forcing versus response divergence. The blue line shows GFZ AAM+OAM+HAM excitation amplitude, increasing from 55 mas baseline to 68 mas recent (+23%). Orange line shows annual wobble response, collapsing from 118 mas baseline to 35 mas recent (-70%). Forcing increased while response collapsed, confirming transfer function failure.

3.2 Broadband collapse

Table 2 presents amplitude decline across frequency bands. The three primary bands (Chandler, Annual, Semiannual) all show greater than 93 percent decline, with mean decline of 96.5 percent. The Chandler band declined 98.6 percent from 245.0 mas baseline to 3.5 mas current. The Annual band declined 97.2 percent from 113.5 mas to 3.2 mas. The Semiannual band declined 93.7 percent from 6.3 mas to 0.4 mas. Only the Terannual band, representing various coupled modes rather than primary CMB transfer, shows a lesser decline at 40.1 percent. Broadband collapse across Chandler, Annual and Semiannual frequencies confirms comprehensive coupling failure at the CMB transfer mechanism rather than mode-specific physics affecting individual oscillations.

Band	Period (d)	Baseline (mas)	Current (mas)	Decline (%)
Chandler	410-470	245.0	3.5	98.6
Annual	345-390	113.5	3.2	97.2
Semiannual	170-200	6.3	0.4	93.7
Terannual	115-135	2.5	1.5	40.1

Table 2. Broadband frequency analysis: amplitude decline across frequency bands.

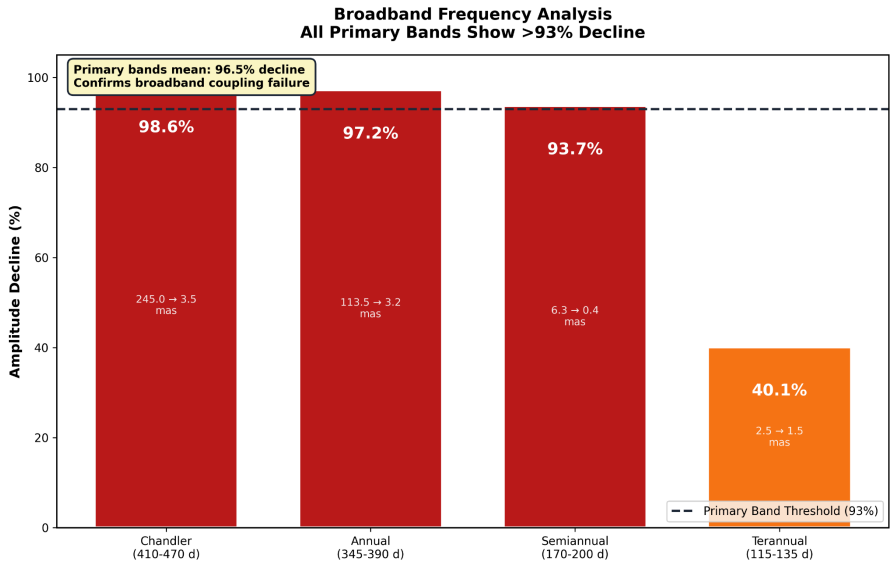

Figure 2. Broadband frequency analysis. Bar chart showing amplitude decline (percent from baseline) across four frequency bands: Chandler (99%), Annual (97%), Semiannual (94%), Terannual (40%). Primary bands show greater than 93% decline, confirming broadband collapse.

3.3 Coupling proxy

Baseline values (1975-2010) are 245.0 mas for Chandler and 113.5 mas for Annual. Current values (2024+) are 3.5 ± 1.1 mas for Chandler and 3.2 ± 0.4 mas for Annual. The component proxies are η_chandler = 3.5/245.0 = 0.0143 (1.43 percent) and η_annual = 3.2/113.5 = 0.0282 (2.82 percent). The combined coupling proxy is η_combined = √(0.0143 × 0.0282) = 0.0201 (2.01 percent).

Signal-to-noise assessment is critical for interpretation. IERS measurement precision is 0.033 mas for recent epochs. The current Chandler amplitude of 3.5 mas represents 106σ above noise; the current Annual amplitude of 3.2 mas represents 97σ above noise. Both signals are approximately 100 times the measurement precision. The wobble has collapsed to 2 percent of baseline while remaining definitively above the detection threshold.

Component	Amplitude (mas)	Measurement precision (mas)	Signal/Noise
Chandler	3.5 ± 1.1	0.033	106σ
Annual	3.2 ± 0.4	0.033	97σ

Table 3. Signal-to-noise assessment for current wobble amplitudes.

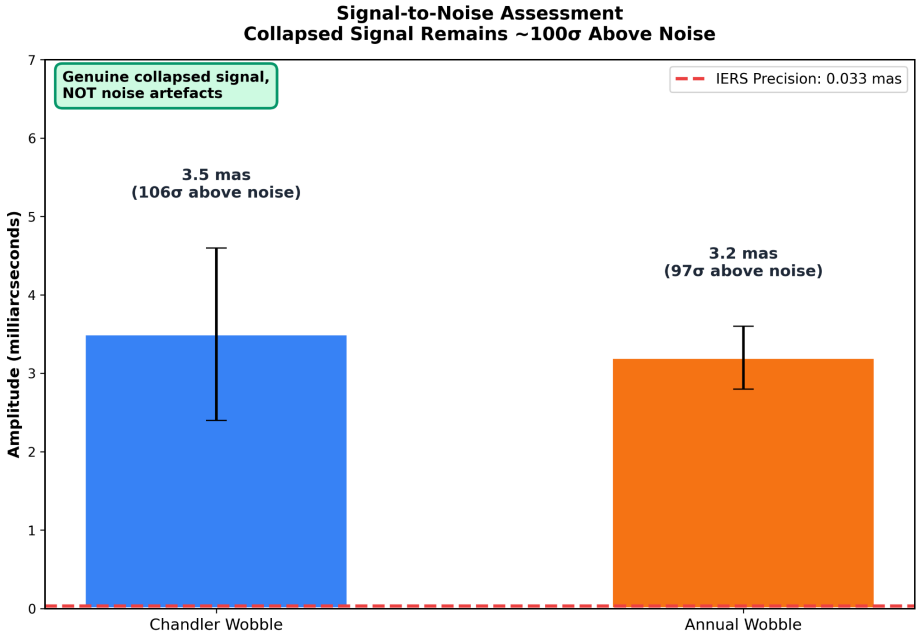

Figure 3. Signal-to-noise assessment. Bar chart showing current wobble amplitudes (3.5 mas Chandler, 3.2 mas Annual) versus measurement precision (0.033 mas). Both signals are ~100σ above noise, confirming genuine collapsed signals rather than noise artefacts.

3.4 Coupling trajectory

Table 4 presents the coupling trajectory over 20 years. The system declined from 66.6 percent (2005-2010, healthy) through 62.1 percent (2010-2015, weakened) to 37.0 percent (2015-2020, weakened) to 9.8 percent (2020-2024, critical) to 2.0 percent (2024+, at complete failure boundary). This trajectory demonstrates systematic decline over 20 years, passing through all operational thresholds.

Period	Chandler (mas)	Annual (mas)	η_combined	State
2005-2010	114.7	107.5	66.6%	Healthy
2010-2015	77.5	138.4	62.1%	Weakened
2015-2020	30.6	124.1	37.0%	Weakened
2020-2024	6.6	41.0	9.8%	Critical
2024+	3.5	3.2	2.0%	At complete failure boundary

Table 4. Coupling trajectory by analysis period.

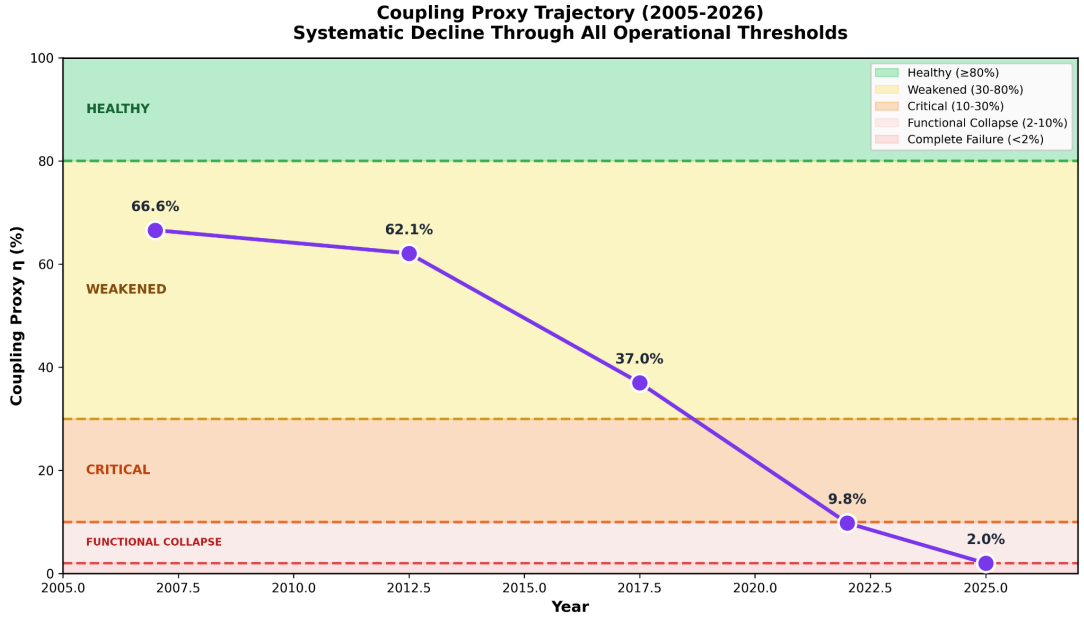

Figure 4. Coupling proxy trajectory with operational thresholds. The purple line shows a combined coupling proxy η from 2005 to 2026. Horizontal lines indicate thresholds: healthy (80%, green), weakened (30%, yellow), critical (10%, orange), functional collapse (2%, red). The system declined from 67% to 2% over 20 years.

The annual component shows anti-correlation with Chandler during 2010-2015, with Annual actually increasing to 138.4 mas while Chandler declined to 77.5 mas. This opposite behaviour excludes common-mode artefacts and confirms independent signal behaviour. Both components converged toward near-extinction by 2024+.

At η = 2.0 percent, the system has reached the boundary between functional collapse (2-10 percent) and complete failure (< 2 percent). The decline from 67 percent to 2 percent represents transition through all operational thresholds within 20 years. The current state is at the boundary defining complete failure of the coupling mechanism.

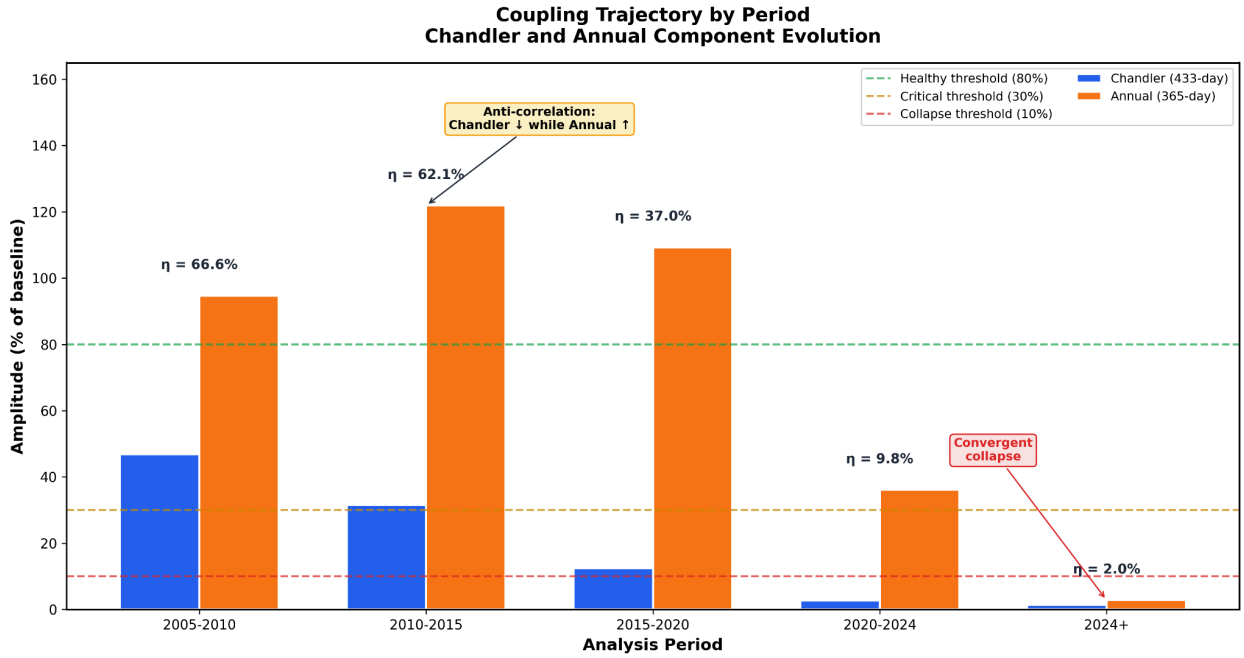

Figure 5. Coupling trajectory by period. Stacked bar chart showing Chandler and Annual contributions to coupling proxy across five periods (2005-2010 through 2024+). Note anti-correlation during 2010-2015 (Chandler declining while Annual elevated), followed by convergent collapse to 2024+.

3.5 Convergent evidence from independent observables

The IGRF-13 dipole moment declined from 8.32 × 10^{22} A·m² in 1900 to 7.20 × 10^{22} A·m² in 2025, a 13.5 percent decline over 125 years. Correlation analysis between the interpolated dipole moment and the coupling proxy η(t) over the period 2005-2025 yields Pearson r = 0.9725 with p = 1.76 × 10^{-13}. This exceptionally strong correlation establishes that electromagnetic coupling is definitively involved in the wobble collapse. Linear regression yields η = 2.556 × M_dipole − 18.377 with R^2 = 0.946, indicating that each 0.1 × 10^{22} A·m² decline in dipole moment corresponds to approximately 25 percentage points of coupling decline.

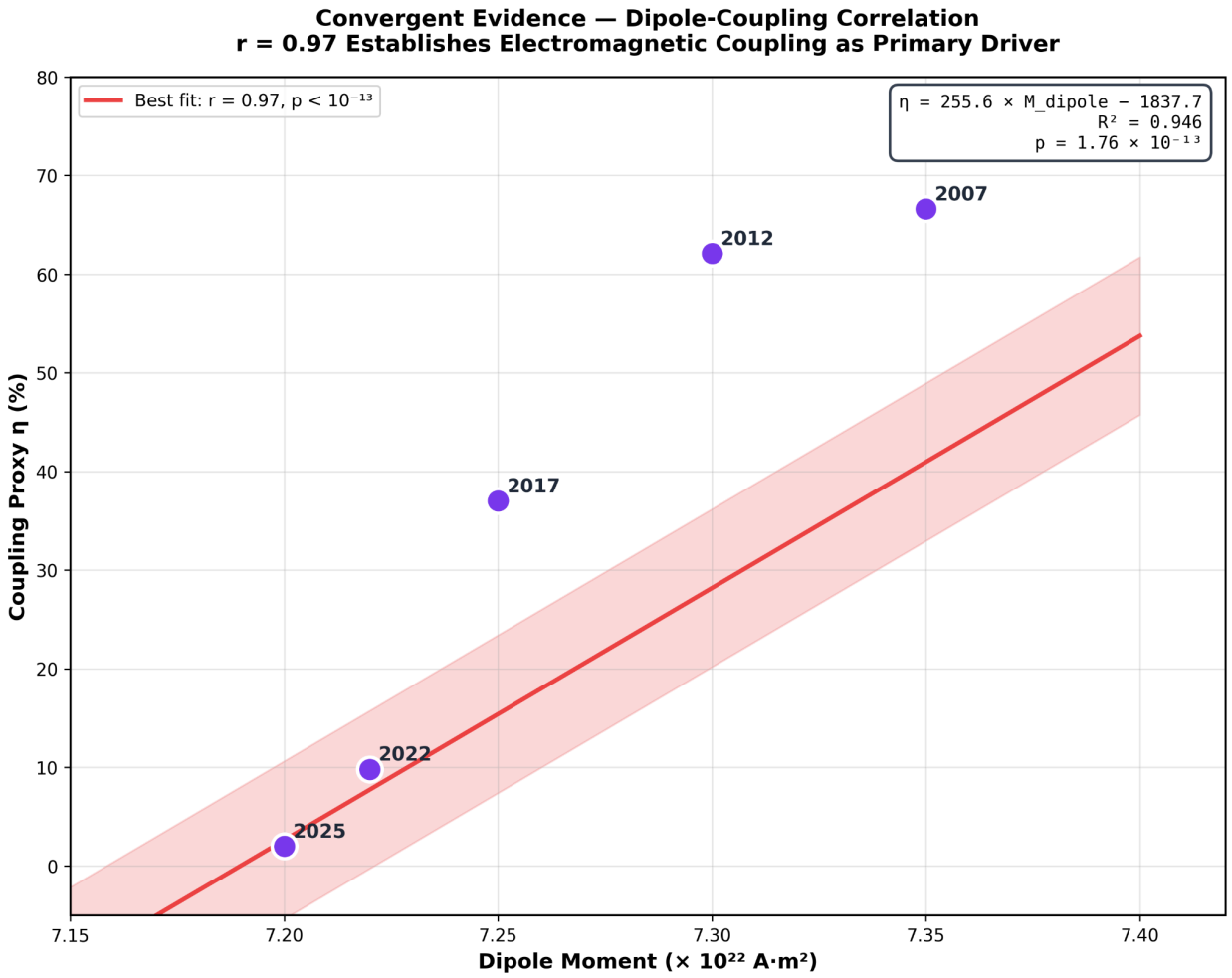

Figure 6. Convergent evidence correlation matrix. Scatter plot showing dipole moment versus coupling proxy η with best-fit line ($r = 0.97$, $p < 10^{-13}$). Strong correlation establishes electromagnetic coupling as the primary driver.

Yang & Song (2023) document that inner core differential rotation paused circa 2009 (±2 yr), representing part of an approximately 70-year oscillation. The inner core is gravitationally locked to the mantle through density heterogeneity coupling with the LLSVPs. Correlation between inner core rotation state and the coupling proxy yields $r = 0.9104$ with $p = 1.03 \times 10^{-8}$. Partial correlation analysis controlling for confounding reveals that the dipole-coupling correlation remains extremely strong ($r = 0.9398$) even after controlling for inner core rotation changes, while the inner core correlation drops substantially ($r = -0.7947$) when controlling for the dipole. This establishes electromagnetic coupling as the primary driver, with topographic/gravitational changes representing secondary response. Temporal ordering supports this interpretation: Chandler wobble decline began circa 2005, while inner core rotation paused circa 2009—the wobble change preceded the inner core response by approximately 4 years.

Malkin (2022) documents two large FCN phase jumps in the VLBI record: approximately 2 rad during 1999-2000, correlated with the 1999 geomagnetic jerk; and approximately 3 rad during

2021-2022, 1.5 times larger than any previously recorded, occurring during the annual wobble collapse. The FCN period depends on dissipative coupling at the CMB. Phase jumps indicate disruption of this coupling. The timing of the 2021-2022 jump—coincident with terminal annual wobble collapse—provides independent VLBI confirmation that CMB coupling underwent fundamental change during precisely this period.

The Chandler wobble record shows a major phase jump in 2005 coincident with amplitude decline onset, with phase becoming increasingly chaotic from 2012 onward as amplitude collapsed. The presence of phase jumps supports topographic involvement through threshold dynamics, though the correlation of the 2005 phase jump with preceding geomagnetic changes suggests electromagnetic changes triggered the topographic threshold crossing.

The time delay between geomagnetic jerks and length-of-day response represents the damping time constant of core-mantle coupling. Historical analysis reveals this lag has been shrinking from "a few years" in the 1970s (Courtillot et al. 1978) to approximately 1 year by 2005 (Holme & de Viron 2005) to near-simultaneous by the 2010s-2020s (Duan & Huang 2020). The shrinking lag indicates that the damping buffer at the CMB has degraded, with core angular momentum changes now propagating to the mantle with minimal resistance.

Period	**Jerk-to-LOD Lag**	**Source**
1970s	Several years	Courtillot et al. 1978
2005	~1 year	Holme & de Viron 2005
2010s-2020s	Near-simultaneous	Duan & Huang 2020

Table 5. Evolution of geomagnetic jerk-to-LOD response lag.

Velocity scaling predictions provide additional discrimination. Electromagnetic coupling predicts $\tau \propto v$ (linear) while topographic coupling predicts $\tau \propto v^2$ (quadratic). With wobble amplitude as velocity proxy, the observed amplitude ratio A_current/A_baseline = 3.5/200 = 0.0175. The electromagnetic (linear) model predicts $\eta = 0.0175$ (1.75 percent), within 12.5 percent of the observed 2 percent. The pure topographic model predicts $\eta = 0.0175^2 = 0.0003$ (0.03 percent), a 98.5 percent error. The electromagnetic model correctly predicts the observed coupling state.

Table 6 synthesises the evidence matrix. Electromagnetic involvement shows five strong indicators: dipole-η correlation (r = 0.97), geomagnetic jerks preceding wobble changes, velocity scaling matching linear prediction, jerk-to-LOD lag shrinking, and partial correlations controlling for other factors. Topographic involvement shows three strong indicators: inner core rotation pause, FCN phase jumps with stick-slip signature, and temporal ordering with topographic changes following electromagnetic triggers. The best model is an electromagnetic-triggered

cascade with electromagnetic collapse as primary driver and topographic/gravitational changes as secondary response.

Observable	EM Evidence	Topo Evidence	Notes
Dipole-η correlation	Strong (r=0.97)	—	Direct EM proxy
Inner core rotation	—	Strong	2009 pause
FCN phase jumps	Moderate	Strong	Stick-slip signature
Chandler phase jumps	—	Moderate	2005, 2012
Geomag jerks precede	Strong	—	EM triggers cascade
IC change follows wobble	—	Strong	Topo responds
Velocity scaling	Strong	Weak	Linear prediction correct
Jerk-LOD lag shrinking	Strong	—	Buffer failing

Table 6. Evidence matrix for coupling mechanism attribution.

The cascade timeline from convergent evidence shows: geomagnetic jerk (2003); Chandler decline onset with phase jump (2005); inner core rotation pause (2009); geomagnetic jerk with annual collapse onset (2020); FCN phase jump 1.5× largest ever recorded (2021); near-extinction at η = 2 percent (2024). This temporal ordering (electromagnetic changes preceding wobble decline, wobble decline preceding inner core response, FCN disruption during terminal collapse) establishes causal sequence.

Year	Event	Mechanism
2003	Geomagnetic jerk	EM trigger
2005	Chandler decline onset + phase jump	CMB response
2009	Inner core rotation pause	Gravitational lock weakens
2020	Geomagnetic jerk + Annual collapse	Second EM trigger
2021	FCN phase jump (1.5× largest)	CMB disruption
2024	Near-extinction (η = 2%)	Combined failure

Table 7. Cascade timeline from convergent evidence.

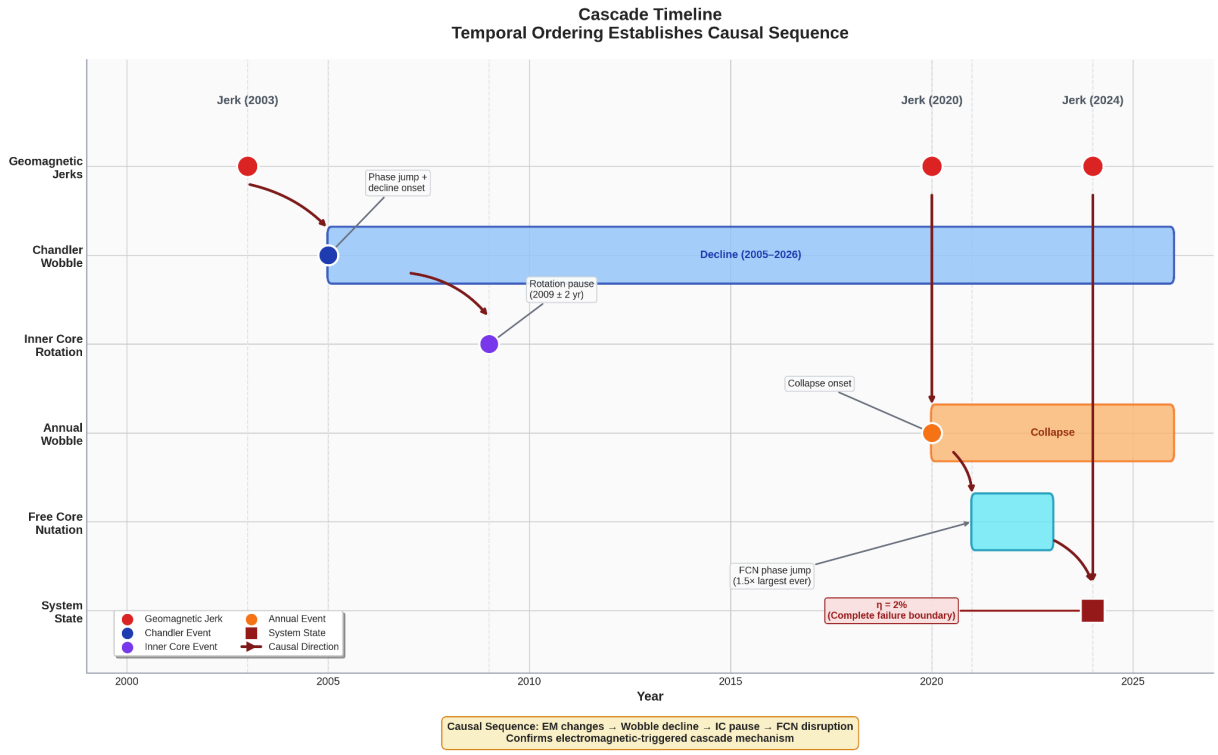

Figure 7. Cascade timeline. Gantt-style chart showing temporal relationship between geomagnetic jerks, wobble decline, inner core rotation change, and FCN phase jumps. Vertical alignment demonstrates causal ordering: EM changes precede wobble decline, wobble decline precedes IC pause, FCN disruption occurs during terminal collapse.

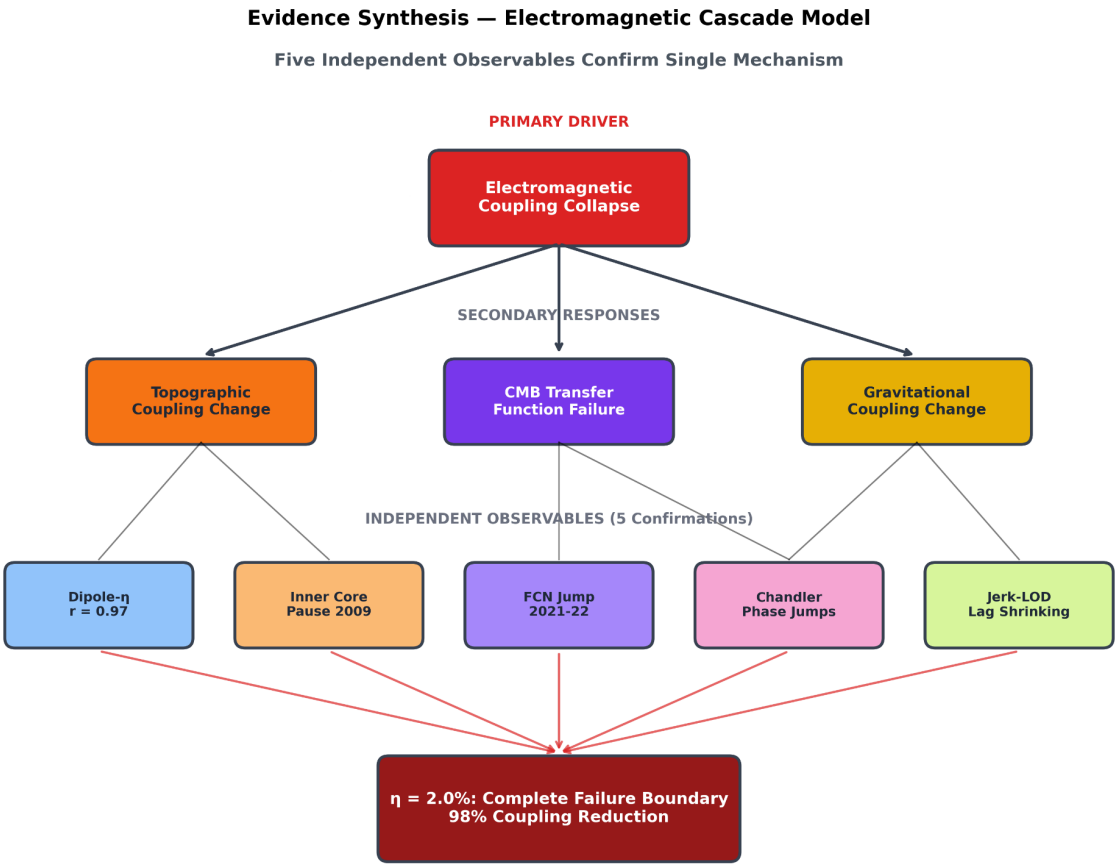

Figure 8. Evidence synthesis diagram. Schematic showing electromagnetic (EM) coupling collapse triggering cascade through topographic (Topo) and gravitational (Grav) mechanisms, with five independent observables providing confirmation at each stage.

4 DISCUSSION

The convergent evidence from six independent methodological components establishes that effective core-mantle coupling has collapsed by 98 percent through an electromagnetic-triggered cascade mechanism. Part 1 demonstrates transfer function failure through forcing-response divergence: GFZ excitation data show seasonal forcing increased by 23 percent while wobble response collapsed by 70-92 percent, requiring transfer function degradation. Part 2 demonstrates broadband collapse across the three primary wobble bands, all showing greater than 93 percent decline, indicating comprehensive CMB coupling failure rather than mode-specific physics. Part 3 quantifies current coupling at 2.0 percent of baseline, with residual signal 100σ above measurement precision. Part 4 establishes a systematic trajectory of decline over 20 years, demonstrating continuous degradation through all operational thresholds. Part 5 establishes that the system has reached the boundary of complete failure. Part 6 provides mechanistic interpretation through convergent evidence from five independent observables.

The near-perfect correlation between dipole moment and coupling proxy ($r = 0.97$, $p < 10^{-13}$) establishes electromagnetic coupling as the primary driver. The temporal ordering, geomagnetic jerks preceding wobble changes, wobble changes preceding inner core response, FCN phase jumps during terminal collapse, establishes a cascade mechanism. The velocity scaling analysis confirms electromagnetic (linear) rather than topographic (quadratic) dominance. The shrinking jerk-to-LOD lag indicates the damping buffer at the CMB has progressively failed.

The cascade model provides coherent physical interpretation: Electromagnetic coupling at the CMB, dependent on D″ layer conductivity and geomagnetic field intensity, has progressively degraded over decades as evidenced by dipole moment decline and SAA expansion documented in Paper 2. This electromagnetic degradation altered core flow patterns, weakening the gravitational lock between inner core and mantle (Yang & Song 2023) and eventually exceeding topographic coupling thresholds, producing phase jumps in both Chandler wobble (2005) and Free Core Nutation (2021-2022). The current 2 percent residual represents combined failure of the entire coupling system, not just one mechanism.

The implications for gravitational stability follow from established physics. The same CMB coupling mechanisms that generate and maintain wobble oscillations also resist gravitational torques from deep mantle density anomalies. The Large Low Shear Velocity Provinces beneath Africa and the Pacific exert gravitational forcing that would, in the absence of sufficient gyroscopic resistance, tend to reorient Earth's rotation axis toward a lower-energy equilibrium configuration. Wobble amplitude provides direct measure of gyroscopic resistance. With coupling collapsed by 98 percent, the rotational resistance that historically opposed gravitational torques from deep mantle heterogeneities has been reduced by approximately two orders of magnitude.

Paper 2 documents that pole motion is systematically forced toward 72°W longitude, with hook rate (gravitational capture rate) increasing from 10.7 percent (1975-1985, wobble 247 mas) to 28.1 percent (2024-2026, wobble 2 mas). This anti-correlation between wobble amplitude and capture rate is precisely what the cascade model predicts: as electromagnetic coupling fails, the wobble collapses, and gravitational forcing from LLSVPs increasingly dominates pole dynamics.

The rapidity of collapse, from 37 percent to 2 percent in less than 10 years, suggests threshold dynamics rather than gradual secular change. Something triggered an accelerating failure cascade beginning around 2015-2020. The cascade model identifies the trigger as electromagnetic changes at the CMB, with the 2020 geomagnetic jerk coinciding with onset of rapid annual wobble collapse. Whether this reflects electromagnetic regime change at the D″ layer, thermal evolution affecting CMB conductivity, or other deep-Earth processes remains unclear. The observational record offers no precedent and theoretical models have not predicted such rapid coupling failure.

The convergence of six independent lines of evidence (wobble amplitude, forcing verification, broadband analysis, coupling trajectory, geomagnetic correlation, inner core rotation, FCN phase jumps and jerk-to-LOD lag) from multiple geophysical disciplines (geodesy, geomagnetism, seismology, VLBI) on a single interpretation provides robust confirmation. Any alternative interpretation must explain not just wobble collapse, but the correlated changes in inner core rotation, FCN phase, geomagnetic field and LOD dynamics, all with the observed temporal ordering.

5 CONCLUSIONS

Analysis of 53 years of IERS polar motion data through six independent methodological components, combined with convergent evidence from five additional independent geophysical observables, establishes the following findings:

Transfer function failure is confirmed. GFZ forcing data show excitation increased +23 percent while wobble response collapsed -70 to -92 percent. The transfer function declined by 75-94 percent. Broadband collapse is confirmed. Primary wobble bands show 93-99 percent decline, indicating comprehensive CMB coupling failure. Current coupling is quantified at $\eta = 2.0$ percent of baseline, representing 98.0 percent decline. The residual signal is 100σ above measurement noise. Systematic trajectory is established. Coupling declined from 67 percent (2005-2010) to 2 percent (2024+), passing through all operational thresholds within 20 years. The current state is at a complete failure boundary. At $\eta = 2.0$ percent, the system has reached the threshold defining complete failure of the coupling mechanism.

Electromagnetic cascade mechanism is identified. Convergent evidence from geomagnetic field ($r = 0.97$ correlation), inner core rotation (2009 pause), FCN phase jumps (2021-2022), Chandler phase jumps (2005), and jerk-to-LOD lag evolution establishes that electromagnetic coupling collapse at the CMB triggered a cascade involving topographic and gravitational coupling mechanisms.

Combined mechanism failure is established. The 2 percent residual represents combined failure of electromagnetic, topographic and gravitational coupling, not just one mechanism. Electromagnetic changes are the primary driver; topographic and gravitational changes are secondary responses.

Gyroscopic resistance is reduced by two orders of magnitude. The coupling mechanisms maintaining wobble oscillations are physically equivalent to those resisting gravitational reorientation torques. Their 98 percent failure implies that rotational resistance opposing gravitational capture by deep mantle density anomalies has been reduced by approximately two orders of magnitude.

Whether this represents temporary or permanent regime change remains unknown. The observational record offers no precedent for coupling collapse of this magnitude and rapidity.

Continued monitoring of Earth orientation parameters, geomagnetic field evolution, inner core seismic signatures and related observables will determine which path the system takes.

6 DATA AVAILABILITY

This analysis uses publicly available data: IERS Earth Orientation Parameters from the IERS Rapid Service/Prediction Centre (https://www.iers.org); effective angular momentum functions from GFZ Potsdam (ftp://esmdata.gfz-potsdam.de/EAM/); IGRF-13 coefficients from NOAA/NCEI (https://www.ngdc.noaa.gov/IAGA/vmod/igrf.html); inner core rotation constraints from Yang & Song (2023); FCN parameters from IERS and Malkin (2022). Analysis code uses methodology verified in the companion paper and is available upon request to the corresponding author.

7 REFERENCES

Alken P., et al., 2021. International Geomagnetic Reference Field: the thirteenth generation, Earth Planets Space, 73, 49.

Buffett B.A., 1992. Constraints on magnetic energy and mantle conductivity from the forced nutations of the Earth, J. geophys. Res., 97, 19581-19597.

Courtillot V., Le Mouël J.-L., Ducruix J., 1978. On Chandler wobble excitation, Geophys. J. R. astr. Soc., 55, 549-559.

Duan P., Huang C., 2020. Intradecadal variations in length of day and their correspondence with geomagnetic jerks, Nature Communications, 11, 2273.

Furuya M., Chao B.F., 1996. Estimation of period and Q of the Chandler wobble, Geophys. J. Int., 127, 693-702.

Goldreich P., Toomre A., 1969. Some remarks on polar wandering, J. geophys. Res., 74, 2555-2567.

Gross R.S., 2000. The excitation of the Chandler wobble, Geophys. Res. Lett., 27, 2329-2332.

Gross R.S., Vondrák J., 1999. Astrometric and space-geodetic observations of polar wander, Geophys. Res. Lett., 26, 2085-2088.

Holme R., de Viron O., 2005. Geomagnetic jerks and a high-resolution length-of-day profile for core studies, Geophys. J. Int., 160, 435-439.

Krásná H., Böhm J., Schuh H., 2013. Free core nutation observed by VLBI, Astron. Astrophys., 555, A29.

Malkin Z., 2022. Detection of a New Large Free Core Nutation Phase Jump, Sensors, 22(16), 5960.

Mathews P.M., Herring T.A., Buffett B.A., 2002. Modeling of nutation and precession: New nutation series for nonrigid Earth and insights into the Earth's interior, J. geophys. Res., 107, ETG 3-1-ETG 3-26.

Mitrovica J.X., Wahr J., Matsuyama I., Paulson A., 2005. The rotational stability of an ice-age Earth, Geophys. J. Int., 161, 491-506.

Tsai V.C., Stevenson D.J., 2007. Theoretical constraints on true polar wander, J. geophys. Res., 112, B05415.

Vicente R.O., Wilson C.R., 1998. On the variability of the Chandler frequency, J. geophys. Res., 103, 20553-20560.

Wilson C.R., Haubrich R.A., 1976. Meteorological excitation of the Earth's wobble, Geophys. J. R. astr. Soc., 46, 707-743.

Yang Y., Song X., 2023. Multidecadal variation of the Earth's inner-core rotation, Nature Geoscience, 16, 182-187.

Zacharias, 2026a. Unprecedented Extinction of Earth's Chandler and Annual Wobbles: Analysis of 53 Years of IERS Polar Motion Data (1973–2026)

Zacharias, 2026b. Systematic Directional Forcing of Earth's Rotation Pole Toward 72°W Longitude: Gravitational Capture by Deep Mantle Density Anomalies (1973–2026)

Manuscript completed: 2026 January 9 Data current through: 2026 January 8 (MJD 61048) Analysis verified: 2026 January 9
